Available online at www.sciencedirect.com
ScienceDirect
Trans. Nonferrous Met. Soc. China 24(2014) 1481−1487
Transactions of Nonferrous Metals Society of China
www.tnmsc.cn

Thermodynamic calculation of high zinc-containing Al−Zn−Mg−Cu alloy

Jun-tao LIU [1, 2], Yong-an ZHANG [1], Xi-wu LI [1], Zhi-hui LI [1], Bai-qing XIONG [1], Ji-shan ZHANG [2]

1. State Key Laboratory of Non-Ferrous Metals and Process, General Research Institute for Non-Ferrous Metals, Beijing 100088, China;
2. State Key Laboratory for Advanced Metals and Materials, University of Science and Technology, Beijing 100083, China

Received 26 September 2013; accepted 3 Dcember 2013

Abstract: Phase fraction and solidification path of high Zn-containing Al−Zn−Mg−Cu series aluminum alloy were calculated by calculation of phase diagram (CALPHAD) method. Microstructure and phases of Al−9.2Zn−1.7Mg−2.3Cu alloy were studied by X-ray diffraction (XRD), differential scanning calorimetry (DSC) and scanning electron microscopy (SEM). The calculation results show that $\eta(MgZn_2)$ phase is influenced by Zn and Mg. Mass fractions of $\eta(MgZn_2)$ in Al−xZn−1.7Mg−2.3Cu are 10.0%, 9.8% and 9.2% for x=9.6, 9.4, 8.8 (mass fraction, %), respectively. The intervals of Mg composition were achieved for $\theta(Al_2Cu)+\eta(MgZn_2)$, $S(Al_2CuMg)+\eta(MgZn_2)$ and $\theta(Al_2Cu)+S(Al_2CuMg)+\eta(MgZn_2)$ phase regions. Al_3Zr, α(Al), $Al_{13}Fe_4$, $\eta(MgZn_2)$, α-AlFeSi, Al_7Cu_2Fe, $\theta(Al_2Cu)$, $Al_5Cu_2Mg_8Si_6$ precipitate in sequence by no-equilibrium calculation. The SEM and XRD analyses reveal that α(Al), $\eta(MgZn_2)$, $Mg(Al,Cu,Zn)_2$, $\theta(Al_2Cu)$ and Al_7Cu_2Fe phases are discovered in Al−9.2Zn−1.7Mg−2.3Cu alloy. The thermodynamic calculation can be used to predict the major phases present in experiment.
Key words: thermodynamic calculation; high-zinc alloy; Al−Zn−Mg−Cu; calculation of phase diagram (CALPHAD)

1 Introduction

Al−Zn−Mg−Cu alloys (7000 series) are extensively used in aeronautical applications, due to their high strength and toughness. In recent decades, three approaches are commonly used to develop Al−Zn−Mg−Cu alloy, i.e. changing the content of main alloying elements (Zn, Mg, Cu), trace elements (Cr, Zr, Sc) additive and reducing impurity element content (Fe, Si) [1]. Through these ways, 7050, 7150, 7055 and 7085 aluminum alloys were developed based on 7075 alloy [2]. Among them, 7055 aluminum alloy owns a higher content of zinc, and 7055-T77 gets attractive combination of properties [3]. Since 1994, several high zinc-containing aluminum alloys like 7055 have been developed, such as 7449, 7136, 7056 and 7095 aluminum alloys [4−8]. The zinc contents of these alloys, especially the latter three alloys, are higher than 8.5%. Research on Al−Zn−Mg−Cu alloys with high Zn has become a hot issue [9−11]. It is known that different contents of Zn, Mg and Cu will play an important role in the formation of $\eta(MgZn_2)$, $T(Al_2Mg_3Zn_3)$, $S(Al_2CuMg)$ and $\theta(Al_2Cu)$ phases, which are common present in Al−Zn−Mg−Cu series alloys. These phases will dominate the balance properties of Al−Zn−Mg−Cu series alloys. In order to know the kinds and amount of these phases, experiment studies have to be used as main approach for materials scientists. Thus, long development cycle and high research cost have to be needed. This traditional experimental method cannot meet the needs of rapid development of aluminum alloy.

Calculation of phase diagram (CALPHAD) method is coupled of phase diagrams and thermochemistry. Now days, it has become a successful and widely applied tool in areas of materials development, including aluminum alloys [12−14]. FARKOOSH et al [15], HE [16], LIU et al [17] assessed formation of phases in multicomponent aluminum alloys, providing support for alloy design. HALLSTEDT [18], MIRKOVIĆ et al [19], HE et al [20], ZHAO et al [21] investigated the solidification paths in Al−Bi−Zn, Al−Si−Mg, Al−Si−Cu−Mg−Ni alloys by thermodynamic simulations, the calculation results were confirmed to be consistent with their experiments,

Foundation item: Project (2012CB619504) supported by the National Basic Research Program of China; Project (51271037) supported by the National Natural Science Foundation of China; Project (2010DFB50340) supported by International Scientific and Technological Cooperation Projects of China
Corresponding author: Yong-an ZHAN; Tel: +86-10-82241065; E-mail: zhangyongan@grinm.com
DOI: 10.1016/S1003-6326(14)63216-7

respectively. Effects of Zn and Mg variations on $\eta(MgZn_2)$ phase, $S(Al_2CuMg)$ phase and T(AlZnMgCu) phase have been computed while the Zn content was in a range of 5.1%−6.7% [22]. The amount of $\eta(MgZn_2)$ phase increased with higher Zn and Mg contents and $S(Al_2CuMg)$ reduced with the increase of Mg content. 7150 aluminum alloy was successfully optimized in the same way, the content of $\eta(MgZn_2)$ phase could be up to 4.5%−6.0%, while the amount of $S(Al_2CuMg)$ phase could be lower than 0.5% [23,24]. There are few thermodynamic calculations about alloy with Zn content higher than 8.5%. Nowadays, many thermodynamic calculation softwares and thermodynamic databases are widely used, such as Thermo-Calc, Pandat, Jmat-Pro, FactSage, MTDATA. Using CALPHAD method, the development cycle can be shortened and research cost can be reduced. The objective of present study is to carry out a thermodynamic calculation for high Zn-containing Al−Zn−Mg−Cu alloy by CALPHAD method.

2 Calculation principle and experiment procedure

2.1 Thermodynamic principle of CALPHAD

Thermodynamics essence of phase diagram is a process to determine the relationship between the target system and alloy composition to obtain the content of each constituent under isothermal and isobaric conditions [25]. When the Gibbs free energy of the target system is the minimum, the system will reach its equilibrium. In this case,

$$G_{\text{tol}} = \sum_{\varphi=1}^{\Psi} n^{\varphi} G_n^{\varphi} = \min \tag{1}$$

where G_{tol} is the total Gibbs free energy of the system; n is the mole fraction of φ phase; Ψ is the total phase number existing in the system; G_n^{φ} is the partial Gibbs free energy of φ phase, which is expressed as

$$G_n^{\varphi} = \sum_i x_i G_i^{0,\varphi} + RT \sum_i x_i \ln x_i + G^{\text{ex},\varphi} \tag{2}$$

where x_i is the mole fraction of component I; $G_i^{0,\varphi}$ is the Gibbs energy of the pure component i with structure φ; R is thermodynamic constant; T is the thermodynamic temperature; $G^{\text{ex},\varphi}$ is the excess Gibbs energy of the phase, which is defined as

$$G^{\text{ex},\varphi} = \sum_{i,j=1(i\neq j}^{n} x_i x_j \sum_{k=0}^{m} L_{(i,j)}^{k} (x_i - x_j)^k + \sum_{i,j,l=1} x_i x_j x_l \sum_{k=i,j,l} L_k \left(x_k + \frac{1 - \sum_{p=i,j,l} x_p}{n}\right) \tag{3}$$

where the first term represents the binary interaction term and the second represents ternary. Optimization method, iterative method and distribution iterative method are used by computer; the composition of each phase can be obtained using Eqs. (1)−(3).

2.2 Materials and thermodynamic model

The compositions of materials calculated are based on Al−9.2Zn−1.7Mg−2.3Cu alloy. The contents of Zn, Mg and Cu are in the ranges of 8.8%−9.6%, 1.3%−2.1% and 1.9%−2.1%, respectively. All of the calculations were processed by thermodynamic calculation software Pandat and its thermodynamic database. $\eta(MgZn_2)$, $\theta(Al_2Cu)$ and $S(Al_2CuMg)$ phases existing in Al−xZn−1.7Mg−2.3Cu (x=8.8, 9.0, 9.2, 9.4, 9.6, mass fraction, %), Al−9.2Zn−yMg−2.3Cu (y=1.3, 1.5, 1.7, 1.9, 2.1, mass fraction, %) and Al−9.2Zn−1.7Mg−zCu (z=1.9, 2.1, 2.3, 2.5, 2.7, mass fraction, %) alloys were calculated by equilibrium model. Solidification paths of Al−9.2Zn−1.7Mg−2.3Cu alloy were calculated using both Scheil model (non-equilibrium model) and ruler model (equilibrium model).

2.3 Experiment procedure

Al−9.2Zn−1.7Mg−2.3Cu alloy was prepared by semi-continuous casting to verify accuracy of thermodynamic calculation. The stainless steel thin-wall pipe was applied as the casting ingot mould and the pouring temperature was 710−720 °C. The ingot was air-cooled to room temperature. The size of the final ingot was 210 mm in diameter and 340 mm in height. The samples were taken at the mid-radius location of the top ingots.

Differential scanning calorimetry (DSC) was performed using NETZSCH STA 409C/CD differential scanning calorimeter. The DSC samples with average mass of about 25 mg were machined from plates to discs with 3 mm in diameter and 1 mm in height. The experiment was performed at a heating rate of 10 °C/min and was carried out from room temperature up to 600 °C. The microstructures were analyzed by scanning electron microscopy (SEM), energy dispersive X-ray spectrometry (EDS) and X-ray diffraction (XRD). The species were ground and polished before analysis.

3 Thermodynamic calculation and experiment results

3.1 Polythermal section of Al–Zn–Mg–Cu phase diagram

Figure 1 shows a calculated isopleth of the Al−Zn−Mg−Cu system (Al−Mg alloys with fixed values of 2.3%Cu, and 8.8%, 9.2%, 9.6%Zn, respectively). The section shows that crystallization of the alloys begins with the solidification of aluminum solid solution (α(Al)). Three important phase regions 5, 11 and 13 are

concerned. $\theta(Al_2Cu)$ phase will be formed in phase region 5, $S(Al_2CuMg)$ will precipitate in phase region 13, and both $\theta(Al_2Cu)$ and $S(Al_2CuMg)$ will precipitate in phase region 11. Region 11 extends to upper left with the reduction of Zn content, which is shown in Fig. 1(b) clearly. Mg compositions corresponding to these three phase regions are shown in Table 1. It reveals that Mg composition ranges are distinctly different for various Zn contents. The Mg composition range narrows down with the increase of Zn content. From the statics listed in Table 1, the phases presented in designed alloy can be deuced. $\eta(MgZn_2)$ and $\theta(Al_2Cu)$ phases will appear in

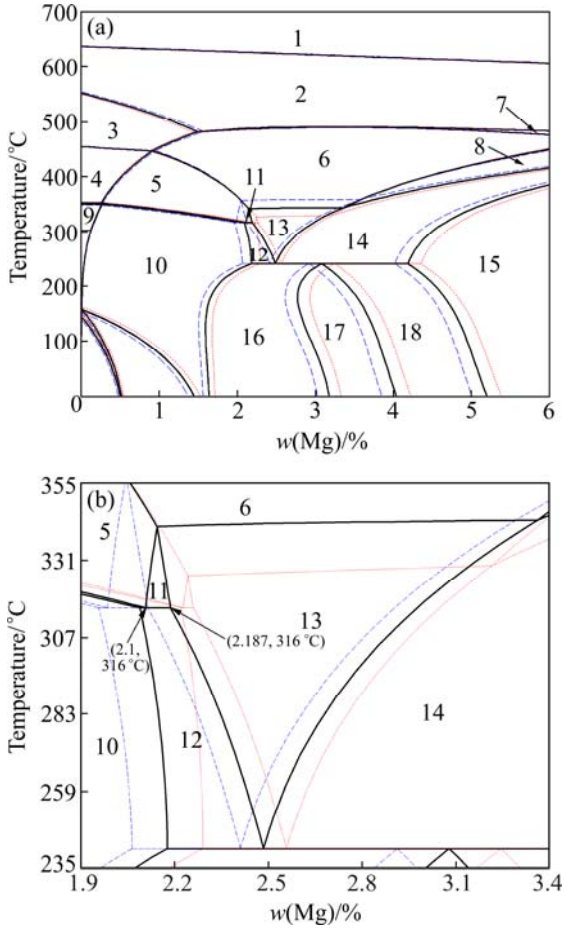

Fig. 1 Calculation polythermal section (a) and its partial enlarged section (b) of Al−Zn−Mg−Cu phase diagram (blue dash line: 8.8% Zn, 0−6% Mg, 2.3% Cu; black line: 9.2% Zn, 0−6% Mg, 2.3% Cu; red dot line: 9.6% Zn, 0−6% Mg, 2.3% Cu): 1—L; 2—L + α(Al); 3—α(Al); 4—α(Al) + $\theta(Al_2Cu)$; 5—α(Al) + $\eta(MgZn_2)$ + $\theta(Al_2Cu)$; 6—α(Al) + $\eta(MgZn_2)$; 7—L + α(Al) + $\eta(MgZn_2)$; 8—α(Al) + $\eta(MgZn_2)$ + $T(Al_2Mg_2Zn_3)$; 9—α(Al) + τ; 10—α(Al) + $\eta(MgZn_2)$ + τ; 11—α(Al) + $\eta(MgZn_2)$ + $\theta(Al_2Cu)$+$S(Al_2CuMg)$; 12—α(Al) + $\eta(MgZn_2)$ + $S(Al_2CuMg)$ + τ; 13—α(Al) + $\eta(MgZn_2)$ + $S(Al_2CuMg)$; 14—α(Al) + $\eta(MgZn_2)$ + $T(Al_2Mg_3Zn_3)$ + $S(Al_2CuMg)$; 15—α(Al) + $T(Al_2Mg_3Zn_3)$ + $S(Al_2CuMg)$; 16—α(Al) + $\eta(MgZn_2)$ + $T(Al_2Mg_3Zn_3)$ + τ; 17—α(Al) + $T(Al_2Mg_3Zn_3)$ + τ; 18—α(Al) + $S(Al_2CuMg)$ + $T(Al_2Mg_3Zn_3)$ + τ

Table 1 Mg composition for three important phase regions

w(Zn)/%	$w(\alpha(Al)+\eta+\theta)$/%	$w(\alpha(Al)+\eta+S+\theta)$/%	$w(\alpha(Al)+\eta+S)$/%
8.8	0.263−1.985	1.985−2.12	2.12−3.565
9.2	0.257−2.1	2.1−2.187	2.187−3.365
9.6	0.252−2.23	2.23−2.26	2.26−3.214

Al−9.2Zn−1.3Mg−2.3Cu, Al−9.2Zn−1.5Mg−2.3Cu, Al−9.2Zn−1.7Mg−2.3Cu, Al−9.2Zn−1.9Mg−2.3Cu alloys; $\eta(MgZn_2)$, $\theta(Al_2Cu)$ and $S(Al_2CuMg)$ phases will appear in Al−9.2Zn−2.1Mg−2.3Cu. To verify this conclusion, these designed alloys are calculated and the results are completely consistent with the deduce.

3.2 Phases in calculated alloys

In order to further investigate the detail of $\eta(MgZn_2)$, $\theta(Al_2Cu)$, $S(Al_2CuMg)$ and $T(Al_2Mg_3Zn_3)$ phases in high Zn-containing Al−Zn−Mg−Cu alloy, mass fraction of each phase was calculated. $\eta(MgZn_2)$, $\theta(Al_2Cu)$, and $T(Al_2Mg_3Zn_3)$ phases appear in these calculated alloys, and $S(Al_2CuMg)$ cannot be found. Due to mole ratio of Zn to Mg is higher than 3, the major Zn-rich phase is $\eta(MgZn_2)$, and the amount of $T(Al_2Mg_3Zn_3)$ is less than 1%. So, only $\eta(MgZn_2)$ and $\theta(Al_2Cu)$ phases are considered. Figure 2 shows mass fraction of $\eta(MgZn_2)$ phase at different temperatures. It can be seen obviously from Fig. 2(a) that $\eta(MgZn_2)$ changing with temperature is almost the same trend for alloys with different Zn contents. Alloys with higher Zn content can obtain more $\eta(MgZn_2)$ phases at the same temperature. The highest fractions of $\eta(MgZn_2)$ are 10%, 9.8%, and 9.2% for alloys with 9.6%Zn, 9.2%Zn, and 8.8%Zn, respectively. Figure 2(b) shows the mass fraction of $\eta(MgZn_2)$ changing with temperature for different Mg contents. $\eta(MgZn_2)$ in alloys with 1.3%Mg and 1.5%Mg decreases gradually with the increase of temperature. However, curves of the alloys with 1.7%Mg, 1.8%Mg, 1.9%Mg are different with 1.3%Mg and 1.5%Mg alloys. The amount of $\eta(MgZn_2)$ decreases gradually when the temperature is above 237 °C, and there is a trough below 237 °C. Figure 2(c) shows the mass fraction of $\eta(MgZn_2)$ in alloys with various Cu contents. The five curves appear to be the same. This implies that $\eta(MgZn_2)$ phases of alloys with fixed Zn and Mg contents are almost the same. The fraction of $\eta(MgZn_2)$ depends on the amount of Zn and Mg.

Figure 3 shows the curves of $\theta(Al_2Cu)$ changing with temperature. It can be seen from Fig. 3(a) that $\theta(Al_2Cu)$ phases at the same temperature are almost same for alloys with different Zn contents, which illustrates that Zn has little influence on $\theta(Al_2Cu)$. Figures 3(b) and 3(c) show that Cu and Mg have opposite effect on θ phase. The alloys with higher Mg

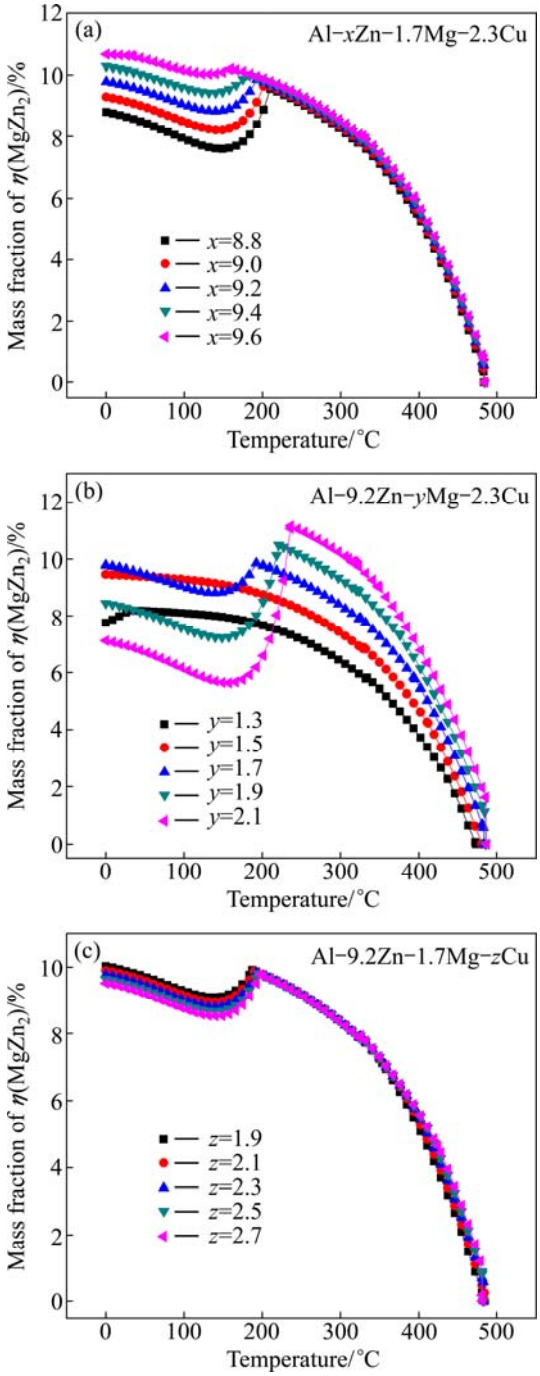

Fig. 2 Curves of mass fraction of $\eta(MgZn_2)$ phase in alloys with temperature

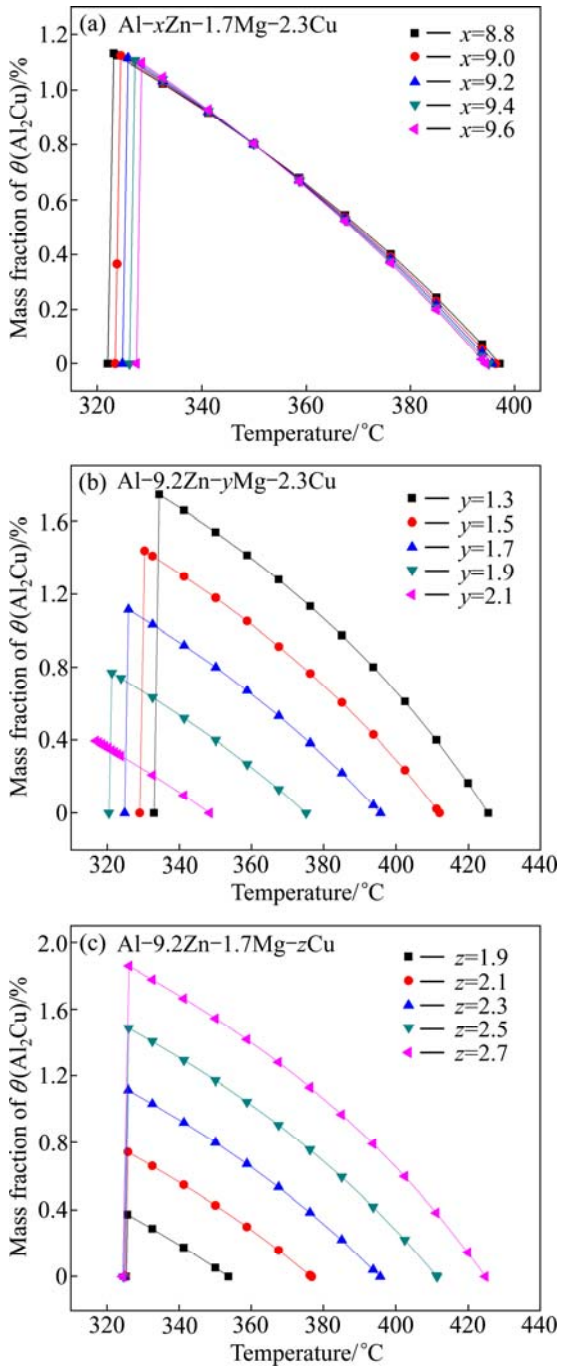

Fig. 3 Curves of mass fraction of $\theta(Al_2Cu)$ phase in alloys with temperature

contents have less fraction of $\theta(Al_2Cu)$ phase with the fixed 9.2%Zn and 2.3%Cu, while the alloys with higher Cu contents can obtain more $\theta(Al_2Cu)$ phase with fixed 9.2%Zn and 1.7Mg. It is well known that $\theta(Al_2Cu)$ virtually does not dissolve Mg, but Al and Cu will substitute for Zn at Zn sublattice of $MgZn_2$ phase. For alloys with fixed Zn and Cu, as the Mg content increases, fraction of $\eta(MgZn_2)$ also increases, thus more Cu is needed to dissolve into $\eta(MgZn_2)$. So, less Al_2Cu will be formed.

3.3 Thermodynamic calculation for solidification paths of Al−9.2Zn−1.7Mg−2.3Cu alloy

Figure 4 shows the curves of solid fraction changing with temperature. Non-equilibrium solidification path is shown as solid line and the equilibrium path is the dash line. Both in equilibrium and non-equilibrium curves, α(Al) begins to precipitate at 627.07 °C. And the non-equilibrium transformation temperature of $\eta(MgZn_2)$ phase is 485.68 °C. The solidus temperature is 413.26 °C for non-equilibrium solidification while the equilibrium

one is 480.6 °C. With the decrease of solidification temperature, Al_3Zr, α(Al), $Al_{13}Fe_4$, η($MgZn_2$), α-AlFeSi, Al_7Cu_2Fe, θ(Al_2Cu), $Al_5Cu_2Mg_8Si_6$ and β-AlFeSi phases are gradually generated in the non-equilibrium solidification process. Al_3Zr, α(Al), $Al_{13}Fe_4$, η($MgZn_2$), Al_7Cu_2Fe, Mg_2Si and η($MgZn_2$) phases precipitate gradually. The solidification temperatures for all phases are also shown in Fig. 4.

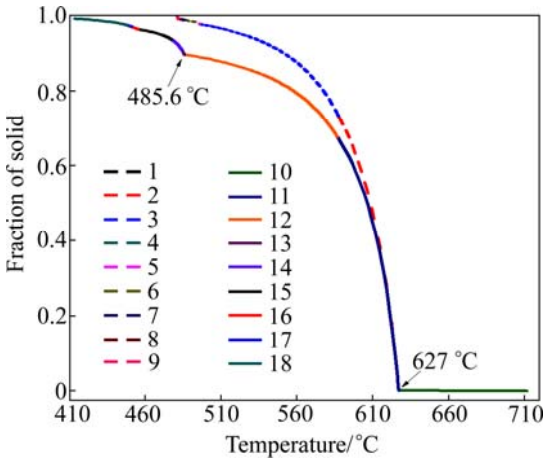

Fig. 4 Solidification path of Al−9.2Zn−1.7Mg−2.3Cu−0.08Fe−0.06Si−0.12Zr (Solid line — Scheil model; Dash line — Equilibrium model): 1—L + Al_3Zr (711.45−627.08 °C); 2—L + Al_3Zr + α(Al) (627.07−587.26 °C); 3—L + Al_3Zr + α(Al) + $Al_{13}Fe_4$ (587.26−494.68 °C); 4—L + Al_3Zr + α(Al) + $Al_{13}Fe_4$ + α-AlFeSi (496.48−495.88 °C); 5—L + Al_3Zr + α(Al) + $Al_{13}Fe_4$ + α-AlFeSi + Al_7Cu_2Fe (495.87−494.85 °C); 6—L + Al_3Zr + α(Al) + α-AlFeSi + Al_7Cu_2Fe (492.8−485.59 °C); 7—L + Al_3Zr + α(Al) + Al_7Cu_2Fe (485.59−483.74 °C); 8—L + Al_3Zr + α(Al) + Al_7Cu_2Fe + Mg_2Si (483.74−481.58 °C); 9—L + Al_3Zr + α(Al) + Al_7Cu_2Fe + η($MgZn_2$) (481.58−480.68 °C); 10—L + Al_3Zr (711.45−627.08 °C); 11—L + Al_3Zr + α(Al) (622.7−586.52 °C); 12—L + Al_3Zr + α(Al) +$Al_{13}Fe_4$ (586.51−485.63 °C); 13—L + Al_3Zr + α(Al) + $Al_{13}Fe_4$ + η($MgZn_2$) (485.62−484.0 °C); 14—L + Al_3Zr + α(Al) + $Al_{13}Fe_4$ + η($MgZn_2$) + α-AlFeSi (483.99− 477.08 °C); 15—L + Al_3Zr + α(Al) + η($MgZn_2$) + Al_7Cu_2Fe (477.08−454.91 °C); 16—L + Al_3Zr + α(Al) + η($MgZn_2$) + Al_7Cu_2Fe + θ(Al_2Cu) (454.91− 450.86 °C); 17—L + Al_3Zr + α(Al) + η($MgZn_2$) + Al_7Cu_2Fe + θ(Al_2Cu) + $Al_5Cu_2Mg_8Si_6$ (450.86−447.75 °C); 18—L + Al_3Zr + α(Al) + η($MgZn_2$) + $Al_5Cu_2Mg_8Si_6$ + β-AlFeSi (447.75−413.26 °C)

DSC test was carried out to verify the accuracy of this calculation result. Figure 5 shows DSC curve of as-cast Al−9.2Zn−1.7Mg−2.3Cu alloy. It shows that there is an obvious exothermic peak at 478.8 °C corresponding to dissolution of low melting point eutectic phase, and no other match peaks can be found. The low melting point eutectic phases are proved to be α(Al)+η($MgZn_2$), which will be discussed further in the next section. The peak temperature is more consistent with the temperature calculated by equilibrium model. This calculated melting temperature of η($MgZn_2$) can be used as an important reference temperature to determine the heat treatment procedures.

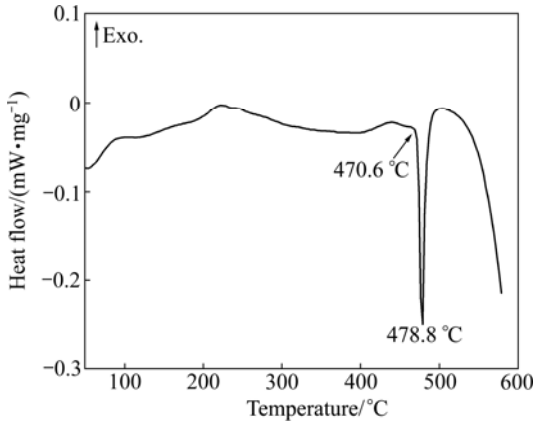

Fig. 5 DSC curve of as-cast Al−9.2Zn−1.7Mg−2.3Cu−0.08Fe−0.06Si−0.12Zr alloy

3.4 Microstructure of Al−9.2Zn−1.7Mg−2.3Cu alloy

Figure 6 shows the XRD curve of Al−9.2Zn−1.7Mg−2.3Cu alloy. Peaks of three phases can be identified, and α(Al), η($MgZn_2$) and θ(Al_2Cu) phases present in actual solidification of Al−9.2Zn−1.7Mg−2.3Cu alloy. The peak intensities of both α(Al) and η($MgZn_2$) phase are high, while poor for θ(Al_2Cu). The other calculated phases are not found in this pattern. The reason maybe is that the amount of these phases is too less to be tested by XRD. According to the XRD results, DSC analysis, and calculation results of solidification, it can be found that both of the non-equilibrium and equilibrium solidification models can be taken as references for solidification. However, the non-equilibrium solidification path is more consistent with actual process without considering diffusion [26].

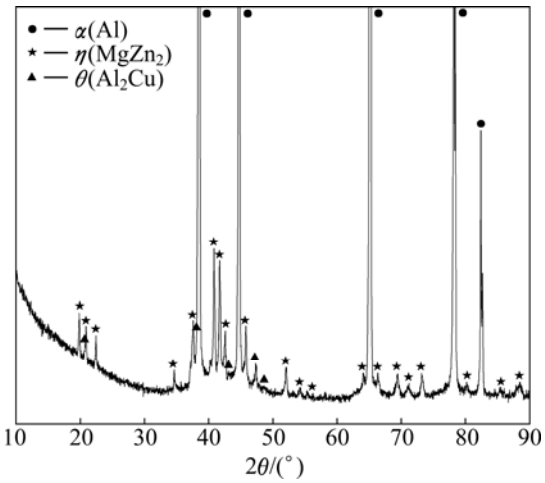

Fig. 6 XRD pattern of Al−9.2Zn−1.7Mg−2.3Cu−0.08Fe−0.06Si−0.12Zr alloy

Analysis of SEM with EDS is employed to further confirm the solidification phases in as-cast Al−9.2Zn−1.7Mg−2.3Cu alloy. The SEM images are shown in Fig. 7. It can be obviously been from Fig. 7(a) that the cast sample presents a typical dendritic microstructure. The white areas are α(Al), and the black coarse phases almost form an network around with fine phases which can be recognized as $MgZn_2$ according to Ref. [26]. The eutectic structure presents as lamellar structure shown in Fig. 7(b). The EDS results are shown in Table 2. Phase A contains Al, Zn, Mg, and Cu, and the mole ratio of Mg to (Al,Cu,Zn) is about 1:2. Al and Cu will substitute for Zn at the Zn sublattice of binary η($MgZn_2$), which can be described as $Mg(Al,Cu,Zn)_2$ [26]. Phases B and D can be recognized as θ(Al_2Cu). Phases C and E are Fe-rich phases which can be identified as Al_7Cu_2Fe. From the analysis, Al−9.2Zn−1.7Mg−2.3Cu consists of primary solution α(Al), $MgZn_2$, $Mg(Al,Cu,Zn)_2$, θ(Al_2Cu) and Al_7Cu_2Fe.

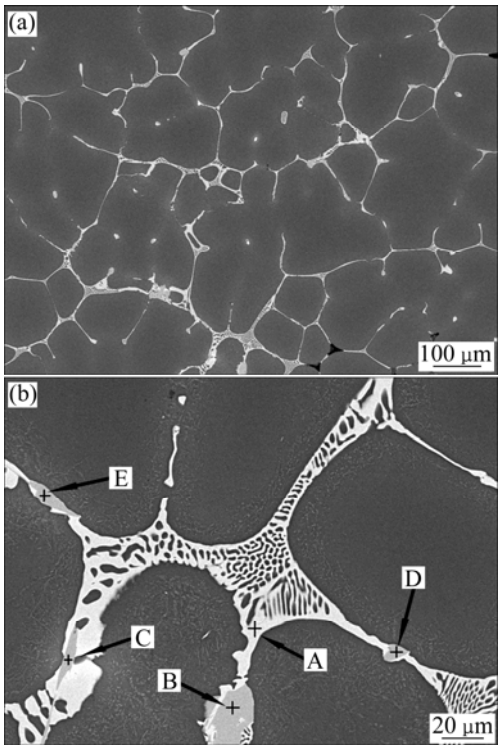

Fig. 7 SEM images of Al−9.2Zn−1.7Mg−2.3Cu−0.08Fe−0.06Si−0.12Zr: (a) Low magnification; (b) High magnification

Table 2 EDS results in Fig. 7(b)

Phase	x(Al)/%	x(Zn)/%	x(Mg)/%	x(Cu)/%	x(Fe)/%
A	23.97	25.45	34.18	16.40	−
B	69.06	1.96	0.85	28.13	−
C	68.30	3.28	−	16.17	12.25
D	68.29	2.25	0.84	28.62	−
E	69.0	1.25	0.68	15.77	13.3

According to the XRD and SEM analyses, both of $MgZn_2$ and $Mg(Al,Cu,Zn)_2$ own the same crystal structure, which can be taken as η($MgZn_2$) phase in the thermodynamic calculation results. The highest fraction of η($MgZn_2$) (see Fig. 2(b)) for Al−9.2Zn−1.9Mg−2.3Cu is 9.8%, which is much more than other phases. So the main phase in calculation is agreement with the experiment results approximately. The minor phases of θ(Al_2Cu) and Al_7Cu_2Fe commonly existing in Al−Zn−Mg−Cu series alloys are also in accordance with the calculation results. However, no other trace phases appearing in calculation results are found in actual experiment, which may be because the phases amount is too less to be found. So it can be concluded that the major calculation phases and minor phases are consistent with the experiment results. The thermodynamic calculation can be recognized as a useful way to the development of Al−Zn−Mg−Cu alloys.

4 Conclusions

CALPHAD method has been applied to thermodynamic calculation for Al−9.2Zn−1.7Mg−2.3Cu series alloys. Al_3Zr, α(Al), $Al_{13}Fe_4$, η($MgZn_2$), α-AlFeSi, Al_7Cu_2Fe, θ(Al_2Cu), $Al_5Cu_2Mg_8Si_6$ and β-AlFeSi are found in calculated non-equilibrium solidification path while η($MgZn_2$), $Mg(Al,Cu,Zn)_2$, θ(Al_2Cu) and Al_7Cu_2Fe present in experimental observation. Thermodynamic calculation results agree with experimental ones to some extent. Mg content intervals of θ(Al_2Cu) + η($MgZn_2$), S(Al_2CuMg) + η($MgZn_2$) and θ(Al_2Cu) + S(Al_2CuMg) + η($MgZn_2$) can provide help for design of aluminum alloy. Besides, high content of Zn or Mg will induce high fraction of η($MgZn_2$), and Cu has little influence on η($MgZn_2$) phase.

References

[1] GEORGE E T, D SCOTT M. Handbook of aluminum: Physical metallurgy and processes [M]. New York: Marcel Dekker, Inc., 2003: 185−194.

[2] ANTIPOV V, SENATOROVA O, TKACHENKO E A, VAKHROMOV R O. High-strength Al–Zn–Mg–Cu alloys and light Al−Li alloys [J]. Metal Science and Heat Treatment, 2012, 53(9−10): 1−6.

[3] CHEN Kang-hua, LIU Hong-wei, ZHANG Zhuo, ZHANG Zhuo, LI Song, TODD IR I. The improvement of constituent dissolution and mechanical properties of 7075 aluminum alloy by stepped heat treatments [J]. Journal of Materials Processing Technology, 2003, 142(1): 190−196.

[4] SAINFORT P, GOMIERO P. 7000 alloy having high mechanical strength and a process for obtaining it: US Patent 5560789 [P]. 1996−10−01.

[5] KAMP N, SINCLAIR I, STARINK M. Toughness-strength relations in the overaged 7449 Al-based alloy [J]. Metallurgical and Materials Transactions A, 2002, 33(4): 1125−1136.

[6] TANAKA M, DIF R, WARNER T. Chemical composition profiles across grain boundaries in T6, T79 and T76 tempered AA7449 alloy

[J]. Materials Science Forum, 2002, 392−406: 1449−1454.
[7] WARNER T, SIGLI C, BES B. Al−Zn−Mg−Cu alloys and products with improved ratio of static mechanical characteristics to damage tolerance: US Patent 7550110B2 [P]. 2009−06−23.
[8] NOWILL C. Investigation of the quench and heating rate sensitivities of selected 7000 series aluminum alloys [D]. Worcester: Worcester Polytechnic Institute, 2007: 1−10.
[9] ZHANG Hui, JIN Neng-ping, CHEN Jiang-hua. Hot deformation behavior of Al−Zn−Mg−Cu-Zr aluminum alloys during compression at elevated temperature [J]. Transactions of Nonferrous Metals Society of China, 2011, 21(3): 437−442.
[10] WANG Gao-song, ZHAO Zhi-hao, ZHANG Yi-hang, CUI Jian-zhong. Effects of solution treatment on microstructure and mechanical properties of Al−9.0 Zn−2.8 Mg−2.5 Cu−0.12 Zr−0.03 Sc alloy [J]. Transactions of Nonferrous Metals Society of China, 2013, 23(9): 2537−2542.
[11] LI Wen-bin, PAN Qing-lin, XIAO Yan-ping, HE Yun-bin, LIU Xiao-yan. Microstructural evolution of ultra-high strength Al−Zn−Cu−Mg−Zr alloy containing Sc during homogenization [J]. Transactions of Nonferrous Metals Society of China, 2011, 21(10): 2127−2133.
[12] SAUNDERS N. The modelling of stable and metastable phase formation in multi-component Al-alloys [C]// Proceedings of 9th International Conference on Aluminium Alloys. Australian: Institute of Materials Engineering Australasia Ltd., 2004: 2−5.
[13] SAUNDERS N, LI X, MIODOWNIK A P, SCHILLÉ J P. Modelling of the thermo-physical and physical properties for solidification of Al-alloys [C]// Light Metals. America: John Wiley & Sons Ltd., 2003: 999−1004.
[14] DU Yong, LIU Shu-hong. ZHANG LI-jun, XU Hong-hui, ZHAO Dong-dong, WANG Ai-jun, ZHOU Liang-cai. An overview on phase equilibria and thermodynamic modeling in multicomponent Al alloys: Focusing on Al−Cu−Fe−Mg−Mn−Ni−Zn system [J]. CALPHAD, 2011, 35(3): 427−455.
[15] FARKOOSH A R, JAVIDANI M, HOSEINI M, LAROUCHE D, PEKGULERYUZ M. Phase formation in as-solid and heat-treated Al−Si−Cu−Mg−Ni alloys: Thermodynamic assessment and experimental investigation for alloy design [J]. Journal of Alloys and Compounds, 2013, 55: 596−606.
[16] HE Jing. Effect of magnesium on precipitated phases in 7085 aluminum alloy based on thermodynamic [J]. Journal of Northeastern University, 2010, 31(s1): 245−249. (in Chinese)
[17] LIU H X, WANG C P, YU Y, LIU X J, TAKAKU Y OHNUMA I, KALNUMA R, ISHIDA K. Experiment investigation and thermodynamic calculation of the phase in the Al−Bi−Sn ternary system [J]. Journal of Phase Equilibrium and Diffusion, 2012, 33(1): 9−19.
[18] HALLSTEDT B. Use of calphad thermodynamics to simulate phase formation during semi-solid processing [C]// Proceedings of the Semi-Solid Processing of Alloys and Composites. Aachen, Germany: Trans Tech Publications Ltd, 2008: 641−646.
[19] MIRKOVIĆ D, GRÖBNER J, SCHMID-FETZER R. Solidification paths of multicomponent monotectic aluminum alloys [J]. Acta Materialia, 2008, 56(18): 5214−5222.
[20] HE Zhi, ZHOU Hao-bin, ZHANG Zhong-yao, LI Lan-yun. The solute redistribution during solidification of Al−Si−Mg alloys [J]. Advanced Materials Research, 2012, 49(7): 396−411.
[21] ZHAO Wei-guang, YE Xi-cong, LIU Wen-jun, GU Ming-chun. Solidification path calculations of Al−Cu−Si alloys in Al-rich corner [J]. Advanced Materials Research, 2012, 503−504: 374−377.
[22] YU Jing-jing, LI Xiao-mei. Modelling of the precipitated phases and properties of Al−Zn−Mg−Cu Alloys [J]. Journal of Phase Equilibria and Diffusion, 2011, 32(4): 350−360.
[23] YU Jing-jing., LI Xiao-mei, YU Xin-quan. Thermodynamic analyses on equilibrium precipitation phases and composition design of Al−Zn−Mg−Cu alloys [J]. Journal of Shanghai Jiao Tong University: Science, 2012, 17(3): 286−290.
[24] HAN Yi, LI Lian, DENG Zhen-zhen, LE Yong-kang, ZHANG Xin-ming. Constituent optimization of Al−Zn−Mg−Cu alloy based on thermodynamic calculation method [J]. The Chinese Journal of Nonferrous Metals, 2011, 21(1): 179−183. (in Chinese)
[25] SAUNDERS N, MIODOWNIK A P. CALPHAD (Calculation of phase diagrams): A comprehensive guide [M]. New York: Pergamon Press, 1998: 47.
[26] XIE Fan-you, YAN Xin-yan, DING Ling, ZHANG Fan, CHEN Shuang-lin, CHU M G, CHANG Y A. A study of microstructure and microsegregation of aluminum 7050 alloy [J]. Materials Science and Engineering A, 2003, 355(1−2): 144−153.

高 Zn 含量 Al−Zn−Mg−Cu 合金的热力学计算

刘俊涛[1,2]，张永安[1]，李锡武[1]，李志辉[1]，熊柏青[1]，张济山[2]

1. 北京有色金属研究总院 有色金属材料制备加工国家重点实验室，北京 100088；
2. 北京科技大学 新金属材料国家重点实验室，北京 100083

摘 要：采用相图计算方法对高 Zn 含量 Al−Zn−Mg−Cu 系高强铝合金进行相分数以及凝固路径的热力学计算，并采用 X 射线衍射(XRD)、差示扫描量热法(DSC)和扫描电镜(SEM)方法对 Al−9.2Zn−1.7Mg−2.3Cu 合金进行组成相分析。结果表明，$\eta(MgZn_2)$受 Zn 和 Mg 含量的影响，在 Zn 含量分别为 9.6%，9.4%，8.8%的 Al−xZn−1.7Mg−2.3Cu 合金中 $\eta(MgZn_2)$含量分别为 10%，9.8%，9.2%，同时通过计算得到了 $\theta(Al_2Cu)+\eta(MgZn_2)$，$S(Al_2CuMg)+\eta(MgZn_2)$和 $\theta(Al_2Cu)+S(Al_2CuMg)+\eta(MgZn_2)$相的 Mg 合金成分区间。Al−9.2Zn−1.7Mg−2.3Cu−Zr 合金依次非平衡地析出 Al_3Zr、α(Al)、$Al_{13}Fe_4$、$\eta(MgZn_2)$、α-AlFeSi、Al_7Cu_2Fe、$\theta(Al_2Cu)$、$Al_5Cu_2Mg_8Si_6$ 和 β-AlFeSi。组织分析结果表明，合金主要由 α(Al)，$\eta(MgZn_2)$，$\theta(Al_2Cu)$和 Al_7Cu_2Fe 组成，计算结果可以预测合金中存在的主要析出相。

关键词：热力学计算；高 Zn 合金；Al−Zn−Mg−Cu；相图计算 **(Edited by Xiang-qun LI)**